

# ASSESSMENT OF A DIFFERENTIAL TOTAL ABSORPTIVITY SOLUTION TO THE RADIATIVE TRANSFER EQUATION AS APPLIED IN THE DISCRETE TRANSFER RADIATION MODEL

*N. W. Bressloff, J. B. Moss, and P. A. Rubini*  
Cranfield University, School of Mechanical Engineering,  
Cranfield, Bedfordshire MK43 0AL, England

*A differential total absorptivity (DTA) solution to the radiative transfer equation is assessed for application in the discrete transfer radiation model (DTRM). The new solution technique treats the source temperature dependence of adsorption explicitly, without the need for spectral integration. Predictions are presented for the radiative intensity across single lines of sight, and for the volumetric source variations in a full DTRM calculation between solid walls. DTA exhibits superior performance relative to a differential total transmissivity solution and the weighted sum of gray gases solution. Additionally, gray gas solutions and a homogeneous isothermal path solution are shown to be unsatisfactory.*

## INTRODUCTION

Radiation modeling is a critical component in the prediction of highly temperature-dependent pollutant formation and wall heat transfer in complex combustion systems. The nature of solution is especially important in coupled CFD heat transfer calculations in which it is necessary to strike a compromise between accuracy and computational effort.

The radiative properties of combustion systems are a complicated function of wavelength, temperature, pressure, composition, and path length. Modeling of these dependencies demands three levels of delineation. First, a global model is required to describe the physics of radiation and how it links to the overall analysis of heat transfer and fluid dynamics. Within a particular model, solution of the radiative transfer equation can then be addressed in a number of ways. Finally, a method is required to represent the radiative properties of the participating media. The analysis is further complicated by the different representations of solid-gas and gas-gas radiation. This article presents an assessment of a differential total absorptivity (DTA) solution technique as applied in the discrete transfer radiation model (DTRM) due to Lockwood and Shah [1].

The DTRM represents one of the most popular methods used for the modeling of radiation in a variety of combustion situations including furnaces [2], combustors [3], and flames [4]. The method is a ray-tracing process that solves the

Received 16 August 1995; accepted 3 October 1995.

The authors are pleased to acknowledge the support of EPSRC (Process Engineering Programme) for the research reported, through Grant GR/H 80088.

Address correspondence to Dr. P. A. Rubini, School of Mechanical Engineering, Cranfield University, Cranfield, Bedfordshire MK43 0AL, England.

### NOMENCLATURE

<i>a</i>	gray-gas polynomial weighting coefficient	<b>Subscripts</b>	
<i>E</i>	mean percentage absolute error	<i>b</i>	black-body quantities
<i>i</i>	radiative intensity, kW/m <sup>2</sup> sr	<i>c</i>	carbon dioxide
<i>i<sub>v</sub></i>	radiative intensity, kW/m <sup>2</sup> sr cm	<i>h</i>	water
<i>k</i>	absorption coefficient, m <sup>-1</sup>	<i>i</i>	species
$\bar{k}$	mean line-strength-to-spacing parameter, cm <sup>-1</sup>	<i>j</i>	spectral band or gray gas component
<i>l</i>	path length, m	<i>m</i>	ray descriptor
<i>P</i>	partial pressure, atm	<i>n, r, r'</i>	computational grid cell
<i>q<sup>-</sup></i>	incident radiative flux, kW/m <sup>2</sup>	<i>N</i>	final cell in path
<i>s, s', s''</i>	distance, m	<i>O</i>	origin of path
<i>S</i>	volumetric radiative source, kW	<i>s</i>	source temperature
<i>T</i>	temperature, K	<i>v</i>	wave number
<i>w</i>	weighting of radiative intensity, sr		
<i>a</i>	absorptivity		
$\underline{y}$	spectral line half-width, cm <sup>-1</sup>	<b>Superscripts</b>	
$\frac{1}{6}$	mean strong line parameter, cm	<i>c</i>	correlated solution
$\Delta A$	area of a surface element, m <sup>2</sup>	<i>T</i>	total property
$\epsilon$	emissivity		
$\sigma$	Stefan-Boltzmann constant, kW/m <sup>2</sup> K <sup>4</sup>		
$\tau$	transmissivity		

radiative transfer equation, RTE, along a discrete set of representative directions from fixed points on solid surfaces. It provides approximations to the radiative flux at solid boundaries and to the contribution made by radiation to the energy equation. When a gray gas approximation is used, solution of the RTE is relatively straightforward. However, the approximation lacks physical realism for many combustion situations that are nongray. Kim et al. [5] demonstrate poor performance of the gray gas assumption in the discrete ordinates radiation model. A homogeneous isothermal path solution, as well as a range of constant absorption-coefficient solutions, are applied in the present article to confirm these observations.

Many models have been developed to represent the nongray behavior of combustion products, and they have been used successfully to solve the RTE. Viskanta and Menguc [6] provide brief descriptions of the models and methods without presenting detailed comparisons of their performance. Some comparisons have been made for the discrete ordinates radiation model. Kim et al. [5] show that the computational time savings offered by gray-band solutions, relative to both narrow- and wide-band solutions, is accompanied by a considerable loss in accuracy in the internal fluxes and radiative source distributions across inhomogeneous slabs between black walls. Song [7] compares the wide-band results from [5] with a weighted-sum of gray gases (WSGG) solution, a modified WSGG solution, and a gray gas solution. The WSGG solutions are shown to model accurately the nongray layers considered. Both [5] and [7] analyze only layers between black walls. In the

DTRM, Docherty and Fairweather [8] compare exponential wide-band and statistical narrow-band solutions, but only for individual lines of sight.

In view of the above discussion, the increasing popularity of the DTRM demands a clear appreciation of the less computationally expensive solution techniques for application in coupled CFD heat transfer calculations. Using a differential narrow-band solution as a basis for comparisons, the assessment of DTA is presented relative to a differential total transmissivity solution, a weighted sum of gray gases solution, a range of constant absorption coefficient solutions, and a homogeneous isothermal path solution. Additionally, gas-gas radiation is distinguished from gas-solid radiation,

First, the various solution algorithms are described, starting with the gray gas formulation in the DTRM. Gas property models are considered next, along with their numerical implementation into the algorithms. Results are then presented for the complete solutions when applied to parabolic temperature profiles characteristic of nonpremixed burning in the range 800-1800 K. Predictions are made of the radiative intensity variation for gas-gas radiation across single lines of sight. The same profiles are then applied to a full DTRM calculation between solid walls, and the volumetric source variation is presented. Both black and gray walls are considered. Only emitting-absorbing-nonscattering media are analyzed comprising two of the principal combustion products,  $\text{CO}_2$  and  $\text{H}_2\text{O}$ .

### SOLUTION METHODS

Following the approach of Siegel and Howell [9], integration of the radiative transfer equation (RTE) along a single line of sight yields the monochromatic intensity

$$i_\nu(s) = i_\nu(0) \exp\left[-\int_0^s k_\nu(s'') ds''\right] + \int_0^s i_{b,\nu}(s') \kappa_\nu(s' \rightarrow s) \exp\left[-\int_{s'}^s \kappa_\nu(s'') ds''\right] ds' \quad (1)$$

The first term represents radiance at the start of a path length that is transmitted across  $s$ . The second term is the sum of energy emitted from intermediate points,  $s'$ , that is then transmitted across the remaining path to  $s$ . Integrating Eq. (1) across the spectrum and substituting for transmissivity,

$$\tau_\nu(s' \rightarrow s) = \exp\left[-\int_{s'}^s k_\nu(s'') ds''\right] \quad (2)$$

yields the integrodifferential equation

$$i(s) = \int_0^\infty (0) \tau_\nu(0 \rightarrow s) d\nu + \int_0^s i_{b,\nu}(s') \frac{\tau_\nu(s' \rightarrow s)}{\delta s} ds' d\nu \quad (3)$$

For a gray, homogeneous medium, Eq. (3) simplifies to a recurrence relation expressing the intensity at the end of a path in terms of that at the start:

$$i_n = i_{n-1}\tau_N + i_{b,N}(1 - \tau_N) \quad (4)$$

where  $\tau_N$  is the total transmissivity.

In Eq. (4) is expanded back to the origin of its path, the intensity at a point is expressed as

$$i_n = i_0 \prod_{r=1}^n \tau_r + \sum_{r=1}^n i_{b,r} \varepsilon_r \prod_{r'=r+1}^n \tau_{r'} \quad (5)$$

The constant absorption coefficient (CAC) solution used below is represented by Eq. (5) with  $\tau_r = e^{-k_l} = (1 - \varepsilon_r)$  and constant values of  $k$ . As a new cell in a path is traversed, the transmissivity product for each upstream cell is multiplied by the transmissivity of the new cell.

The ray-tracing process in the DTRM employs Eq. (5)—or Eq. (4) on a cell-by-cell basis—to evaluate incident radiative fluxes,

$$q^- = \sum_{m=1}^M w_m i_m \quad (6)$$

and radiative source terms,

$$AS = \sum_{\text{all rays}} w \Delta i \Delta A \quad (7)$$

where  $\Delta i$  represents the change in intensity of a ray traversing the control volume. Each ray is assumed to occupy a “pencil” equal to the projection of the area,  $\Delta A$ , of the surface element from which it is launched. The  $i_m$  in Eq. (6) are the incident radiative intensities evaluated as the final value along each path from Eq. (5). The summation in Eq. (6) is performed for ray directions representing the solid-angle hemisphere, whereas in Eq. (7) it is for all rays crossing a particular control volume. The weighting coefficients,  $w$ , in Eqs. (6) and (7) are functions of ray directions and the solid angles represented by each ray. They are also dependent upon the alignment of the axes used to discretize the hemispherical solid angle relative to a solid surface [10].

The initial intensity at the origin of every path is

$$i_0 = \frac{[\varepsilon_0 \sigma T_0^4 + (1 - \varepsilon_0)q^-]}{\pi} \quad (8)$$

Since this is dependent on the initial intensities from other solid locations within the domain, the calculation procedure is iterative.

Although the gray gas assumption is computationally attractive, the spectrally dependent nature of emission and absorption make it physically unrealistic. Equations (4) and (5) do not take into account the preferential self-absorption of gases

due to the nongray distribution of absorption and emission lines. For inhomogeneous, nonisothermal paths, the use of total properties in Eq. (4) underestimates absorption, since high absorptivity in particular regions of the spectrum is averaged across the whole spectrum.

Other solution techniques are now described, all derived from Eq. (3), which address the spectral dependence of radiative intensity. A representative value of a property,  $\phi$ , across a path is described by  $\phi_{a \rightarrow b}$ , where  $a$  and  $b$  signify the initial and final elements in the path, respectively.

**Differential Banded Transmissivity (DBT) Solution**

Rewriting Eq. (5), the spectrally correlated intensity across a bandwidth  $\Delta \nu$  is

$$i_\nu^c = \frac{1}{\Delta \nu} \int_{\nu - \Delta \nu/2}^{\nu + \Delta \nu/2} \left[ i_\nu(0) \prod_{r=1}^n \tau_{\nu,r} + \sum_{r=1}^n \left( i_{b,\nu,r} \varepsilon_{\nu,r} \prod_{r'=r+1}^n \tau_{\nu,r'} \right) \right] d\nu \quad (9)$$

The high-resolution structure of the spectrum prohibits a complete representation of the correlation between intensity and absorptivity for engineering calculations. However, Taine [11] demonstrates poor performance of a noncorrelated solution,

$$i_n = \sum_{j=1}^J \left[ i_{0,j} \prod_{r=1}^N \bar{\tau}_{j,r} + \sum_{r=1}^N \left( \bar{i}_{b,j,r} \bar{\varepsilon}_{j,r} \prod_{r'=r+1}^N \bar{\tau}_{j,r'} \right) \Delta \nu \right] \quad (10)$$

where the strength, shape, and distribution of individual lines are modeled by band descriptions of the spectrum, and mean values of intensity and transmissivity are used for each band.

The correlated solution focuses on the recurrence interpretation of the RTE. If, however, the differential transmissivity in Eq. (3) is expanded, for each spectral band, as a finite difference at all upstream locations, the intensity becomes

$$i_n = \sum_{j=1}^J \left[ i_{0,j} \bar{\tau}_{0 \rightarrow n,j} + \sum_{r=1}^n \bar{i}_b(T_s, \nu_j) (\bar{\tau}_{r \rightarrow n,j} - \bar{\tau}_{r-1 \rightarrow n,j}) \Delta \nu_j \right] \quad (11)$$

where the transmissivity difference across an upstream cell is evaluated for paths from the leading and trailing edges of that cell. The black-body intensity,

$$\bar{i}_b(T_s, \nu_j) = \frac{2C_1 \nu_j^3}{e^{C_2 \nu_j / T_s} - 1} \quad (12)$$

is evaluated at the centre of a band and midway between each path origin.  $C_1$  and  $C_2$  are Planck's first and second constants, respectively. Nonuniformities are treated by either scaling the band parameters used to calculate the transmissivity, or by evaluating mean thermodynamic properties for an equivalent homogeneous, isothermal path. The transmissivity for bands comprising more than one species is calculated as the product of the individual species transmissivities.

The first term in Eq. (11) represents the gas transmission of solid wall radiation. The initial intensity of the  $j$ th band is

$$i_{0,j} = \varepsilon_0 \bar{i}_{b,j} \Delta \nu + \frac{(1 - \varepsilon_0) M}{\pi} \sum_{m=\setminus} E w_m \bar{i}_{m,j} \quad (13)$$

where the summation represents the total incident radiation within the band for all rays.

### Differential Total Transmissivity (DTT) Solution

If the order of integration is reversed in Eq. (3), the spectrally resolved transmissivities are replaced by total transmissivities,

$$\tau_{r \rightarrow n}^T(\bar{T}, \bar{p}_c, \bar{p}_h, l) = \frac{\int_0^\infty i_b(T_s, \nu) \tau_{r \rightarrow n}(T, \bar{p}_c, \bar{p}_h, l, \nu) d\nu}{\int_0^\infty i_b(T_s, \nu) d\nu} \quad (14)$$

and the differential total transmissivity solution is expressed as

$$\begin{aligned} i_n = & i_0 \tau_{0 \rightarrow n}^T(\bar{T}_{0 \rightarrow n}, \bar{p}_{c,0 \rightarrow n}, \bar{p}_{h,0 \rightarrow n}, l_{0 \rightarrow n}) \\ & + \sum_{r=1}^n i_b(T_{r-1/2}) \left[ \tau_{r \rightarrow n}^T(\bar{T}_{r \rightarrow n}, \bar{p}_{c,r \rightarrow n}, \bar{p}_{h,r \rightarrow n}, l_{r \rightarrow n}) \right. \\ & \left. - \tau_{r-1 \rightarrow n}^T(\bar{T}_{r-1 \rightarrow n}, \bar{p}_{c,r-1 \rightarrow n}, \bar{p}_{h,r-1 \rightarrow n}, l_{r-1 \rightarrow n}) \right] \quad (15) \end{aligned}$$

To calculate the total radiative properties for nonhomogeneous, nonisothermal paths, Grosshandler [12] recommends concentration-weighted temperatures and partial pressures in the total transmittance nonhomogeneous (TTNH) model:

$$\bar{T}_{s' \rightarrow s} = \frac{\int_{s'}^s [p_w(s'') + p_c(s'')] ds''}{\int_{s'}^s \{ [p_w(s'') + p_c(s'')] / T(s'') \} ds''} \quad (16)$$

$$\bar{p}_{i,s' \rightarrow s} = \frac{\int_{s'}^s [p_i(s'')]^2 / T(s'') ds''}{\int_{s'}^s \{ [p_i(s'')] / T(s'') \} ds''} \quad (17)$$

Within the TTNH model a correction is applied to the transmissivities in order to account for the different temperature dependence in Eq. (14) of the black-body intensity and the total transmissivity.

### Differential Total Absorptivity (DTA) Solution

The corrections in the TTNH model can be avoided if Eq. (3) is rewritten as

$$i(s) = \int_0^\infty i_\nu(0)[1 - \alpha_\nu(0 \rightarrow s)] d\nu - \int_0^\infty i_{\nu}^{r,s}(\nu) \frac{e^{-\nu s}}{\delta s} ds \quad (18)$$

and if a total absorptivity is defined as

$$\alpha_{r \rightarrow n}^T(T_s, \bar{T}, \bar{p}_c, \bar{p}_h, l) = \int_0^\infty i_b(T_s, \nu) \alpha_{r \rightarrow n}(T_s, \bar{T}, \bar{p}_c, \bar{p}_h, l, \nu) d\nu / \int_0^\infty i_b(T_s, \nu) d\nu \quad (19)$$

Now, the source temperature dependence of absorption is treated explicitly and the differential total absorptivity solution is given by

$$i_n = i_0 \left[ 1 - \alpha_{0 \rightarrow n}^T(T_0, \bar{T}_{0 \rightarrow n}, \bar{p}_{c,0 \rightarrow n}, \bar{p}_{h,0 \rightarrow n}, l_{0 \rightarrow n}) \right] + \sum_{r=1}^n i_b(T_{r-1/2}) \left[ \alpha_{r-1 \rightarrow n}^T(T_{r-1/2}, \bar{T}_{r-1 \rightarrow n}, \bar{p}_{c,r-1 \rightarrow n}, \bar{p}_{h,r-1 \rightarrow n}, l_{r-1 \rightarrow n}) - \alpha_{r \rightarrow n}^T(T_{r-1/2}, \bar{T}_{r \rightarrow n}, \bar{p}_{c,r \rightarrow n}, \bar{p}_{h,r \rightarrow n}, l_{r \rightarrow n}) \right] \quad (20)$$

In the DTT solution, transmissivities are evaluated from the trailing edge of each element along a path as a function of the mean temperature for that path. These transmissivities are then used in the finite-difference calculation for the leading edge of the adjacent element. In contrast, the source temperature dependence of absorption in the DTA solution requires that both trailing- and leading-edge absorptivities are evaluated for each element as a function of each element's temperature,  $T_{r-1/2}$ , as well as the mean thermodynamic properties for the path. The computational penalty of this double calculation is approximately equal to that for the corrections required in the DTT solution.

### Weighted Sum of Gray Gases (WSGG) Solution

It can be shown [13] that Eq. (10) also represents the solution for the WSGG solution in the band summation is replaced by a summation for each gray gas, and if the black-body intensity is premultiplied by the corresponding weighting coefficients. The initial intensity of the  $j$ th gray gas is

$$i_{0,j} = \frac{a_j(T_0) \varepsilon_0 \sigma T_0^4 + [1 - \varepsilon_0] \sum_{m=1}^M w_m i_{m,j}}{\pi} \quad (21)$$

where the summation represents the total incident intensity for the  $j$ th gas.

### Homogeneous Isothermal Path Solution (HIP)

The evaluation of all downstream transmissivities due to upstream emission can be avoided by replacing every set of downstream cells by equivalent homogeneous paths. **Alternatively**, this equivalence can be applied to every path such that the intensity at the end of a line of sight is due to emission from a single homogeneous path, combined with the transmission of initial intensity across that path. The latter description represents the HIP solution.

## GAS PROPERTY MODELS

A hierarchy of gas property models can be described based upon the level of spectral resolution employed. At the highest end of this hierarchy for molecular gases are line-by-line models [11], which use high-resolution spectroscopic data to generate integrated line intensities and spectral absorptivities. Despite their high accuracy, calculation times are prohibitive for engineering problems, making line-by-line models unsuitable for the present study. However, the data generated by line-by-line models are used, together with experimental data, to calculate mean band parameters for narrow- and wide-band models. Of the various narrow-band models, the single line group (SLG) method due to Ludwig et al. [14] is used here (with the differential banded transmissivity solution) as the basis for comparisons. Whereas narrow-band models typically divide the spectrum into  $25\text{-cm}^{-1}$  intervals, wide-band models require over an order of magnitude fewer divisions [15].

Many other gas property models do not treat the spectral variation of absorptivity explicitly, since they employ curve-fitting strategies to spectrally calculated total properties. Of these, the weighted sum of gray gases model [16] is especially useful, since it links the physical realism of Beer's law with the simplicity of the gray gas approximation. Other curve-fitting models—also known as total absorptivity-emissivity models—include those due to Modak [17] and Leckner [18].

Curve fits to mean absorption coefficient data have also been made by Hubbard and Tien [19].

The single gray gas approximation, which assumes a constant absorption coefficient across an inhomogeneous path, is at the lowest end of the hierarchy.

### Statistical Narrow-Band Model

Narrow-band models describe the spectral variation of radiative properties by assuming that the distribution of lines, their shape, and their intensity can be represented mathematically. According to these representations, the mean transmissivity within a band can be calculated. The Goody statistical model assumes that lines within a band are randomly located. If line strengths and widths are assumed to be equal, the mean band transmissivity for species  $i$  is then given by

$$\bar{\tau}_{\nu,i} = \exp \left[ -(\bar{k}_{\nu,i} P_i l) \left( \frac{1 + \bar{k}_{\nu,i} \bar{\delta}_{\nu,i} P_i l}{4\bar{\gamma}_{\nu,i}} \right)^{-1/2} \right] \quad (22)$$

Ludwig et al. [14] apply an **approximation** to the optical depth, **which** accounts for combined **Doppler and collision broadening**. Alternative **narrow-band models** are described elsewhere [20].

For a single homogeneous element, the band transmissivity is evaluated as the product of transmissivities for all species. Band transmissivities for nonuniform paths are calculated by using an equivalent homogeneous, isothermal path. This is achieved through the calculation of effective thermodynamic properties by Eq. (16) and (17) or of scaled band parameters using, for example, Curtis-Godson scaling [9].

### Total Absorptivity-Emissivity Models

Curve-fitting models are designed to calculate radiative properties for homogeneous, isothermal media. However, they can be applied to nonuniform media using differential total property solutions or equivalent homogeneous path approximations. Modak's model [17], incorporating Chebyshev polynomial curve fits to wide-band total emissivity data, is used for the present analysis. The total absorptivity is evaluated from

$$\alpha^T = \varepsilon^T \left( \frac{\bar{T}}{T_s} \right)^{0.65 - 0.2 p_w / (p_w - p_c)} \quad (23)$$

The method has been derived for the following range of gas parameters:

$$\begin{aligned} 300 < T < 2,000 \text{ K} \\ 0.0011 \leq p < 1.0 \text{ atm} \\ 0.0011 \leq pl < 5.989 \text{ atm m} \end{aligned} \quad (24)$$

### Weighted Sum of Gray Gases Models

Weighted sum of gray gases models comprise curve fits—normally to total emissivity data—assuming the real gas to be composed of a number of gray gases with windows in the spectrum represented by a single clear gas. Total emissivity is defined by

$$\varepsilon = \sum_{j=0}^J a_j(T) (1 - e^{-k_j pl}) \quad (25)$$

where absorption coefficients,  $k_j$ , independent of temperature are assumed and the temperature dependence is carried by polynomial weighting factors,  $a_j(T)$ . The coefficients for each gas are applied in the WSGG solution described in Eq. (10). Values have been generated for absorption and polynomial coefficients by many authors [21]. Truelove's coefficients [22] are adopted in the present analysis, since they are derived from the narrow-band Ludwig data. They are tabulated for the

following conditions:

$$\begin{aligned} 600 < T < 2,400 \text{ K} \\ 0.01 \leq l < 10.0 \text{ m} \end{aligned} \quad (26)$$

## RESULTS AND DISCUSSION

It is impractical to address all radiative property dependencies in a single article. Therefore, only two temperature profiles are considered: a parabolic maximum varying between 800 and 1,800 K—configuration A—and a parabolic minimum varying between 1,800 and 800 K—configuration B. In both cases the homogeneous mixture comprises only CO<sub>2</sub> and H<sub>2</sub>O in the ratio 1:2, and the total path length of 1.0 m is divided into 20 equal elements.

First, comparisons are made without the interaction of solid boundaries. A single line-of-sight calculation is made for the intensity variation across the two configurations described above. Second, the same configurations are adopted for a one-dimensional property variation with solid wall temperatures equal to the endpoint values of the parabolic profiles. Both black ( $s = 1.0$ ) and low-emissivity gray walls ( $\epsilon = 0.25$ ) are considered. In these cases volumetric sources are evaluated in a full discrete transfer radiation model calculation. Sixteen rays are launched from each side of the slab.

The mean absolute percentage errors relative to the differential banded transmissivity solution are evaluated as

$$E = 100 \frac{\sum_{n=1}^N |I_{\text{DBT},n} - f_n|}{N} \quad (27)$$

where  $I$  represents radiative intensity or volumetric radiative sources. Table 1 summarizes the permutations of solution algorithms and gas property models, and errors are presented in Table 2.

Table 1. Permutations of solution methods and gas property models

DBT	Differential banded transmissivity solution using the SLG narrow-band model due to Ludwig et al.
DTT	Differential total transmissivity solution using Modak's total emissivity data
DTA	Differential total absorptivity solution using Modak's total emissivity data
WSGG	Weighted sum of gray gases solution using Truelove's coefficients
HIP	Homogeneous isothermal path solution using the SLG narrow-band model due to Ludwig et al.
CAC	Constant absorption coefficient solution

Table 2. Mean absolute percentage errors relative to DBT solution

	DTT	DTA	WSGG	HIP
A—line of sight	5.93	5.06	11.35	27.22
B—line of sight	14.77	10.57	21.80	18.04
A—solid wall ( $e = 1.0$ )	29.34	15.56	16.10	69.15
A—solid wall ( $e = 0.25$ )	16.69	12.60	21.28	61.04
B—solid wall ( $e = 1.0$ )	9.49	6.74	20.39	56.63
B—solid wall ( $e = 0.25$ )	20.33	20.76	10.19	32.41

### Configuration A — Single Line of Sight

The radiative intensity variation across configuration A—shown in Figure 1—initially increases with temperature as the hotter elements emit more than they absorb. However, the intensity continues to increase beyond the midpoint of the configuration but at a decreasing rate. Absorption by the increasingly cooler gas only rises above further emission about three-tenths from the end of the line of sight.

The CAC solutions are shown for absorption coefficients between 0.25 and 0.75. Although it is possible to identify a single absorption coefficient that yields the intensity at the end of the line of sight, none of them predicts the complete intensity variation accurately. Similarly, the HIP solution predicts a good final value but has large errors elsewhere.

The WSGG solution has a slightly larger final error than the HIP solution, but produces a better overall prediction of the intensity variation.

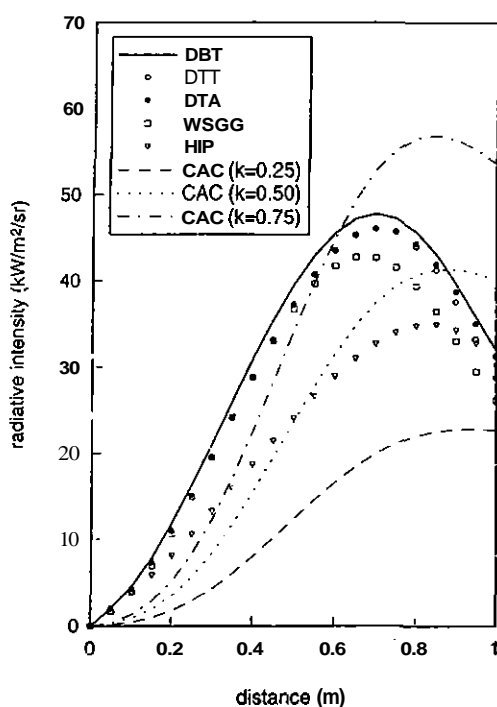


Figure 1. Radiative intensity across configuration A.

Both total property solutions follow the DBT solution very closely for the majority of the path. However, the DTT solution overpredicts absorption at the end of the line of sight. The best performance is produced by the DTA solution, with a mean percentage error of 5.06%.

### Configuration B — Single Line of Sight

In configuration B the hot gas at the start of the path emits more than it absorbs—cf. Figure 2. Absorption soon increases above emission to yield a decreasing intensity variation for approximately the next 50% of the path. Then the increasingly hotter gas reverses the process again and the intensity increases to its largest value at the end of the line of sight.

The same CAC solutions again fail to capture the shape of the intensity variation. In contrast, the HIP solution exhibits good accuracy for the first half of the path. It is expected that the process of averaging properties without adopting a differential representation of the RTE leads to larger errors across the lengthening nonuniform path.

The relative performance between the differential total property solutions and the WSGG solution is the same as it is for configuration A. However, the errors in each case are approximately double the previous values. This is due to the difficulty of capturing the source temperature dependence of absorption, combined with the fact that, in configuration B, the whole path "sees" the hot gas at the start of the path.

### Configuration A with Solid Walls

Figures 3 and 4 show the radiative source variation across configuration A between solid walls that are black ( $e = 1.0$ ) and gray ( $e = 0.25$ ), respectively. Both

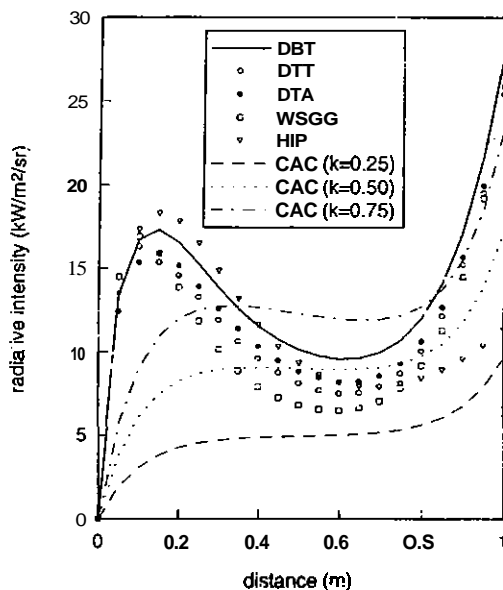


Figure 2. Radiative intensity across configuration B.

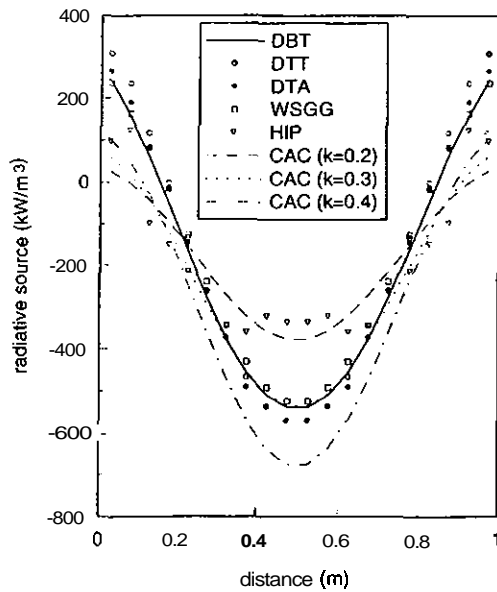


Figure 3. Radiative source across configuration A bounded by solid walls (emissivity = 1.0).

walls are at 800 K. The radiative source represents a balance between absorption and emission, and is considered positive for a cell that is an overall absorber. In contrast to the single lines of sight, each element "sees" radiation from all other elements as well as from the walls.

In both cases the gas adjacent to the walls is a net absorber while the bulk core is a net emitter. The hot gas at the center of the slab is the strongest emitting region. The main difference between the two cases is that the high reflection of the low-emissivity walls produces a higher level of absorption throughout the gas. For

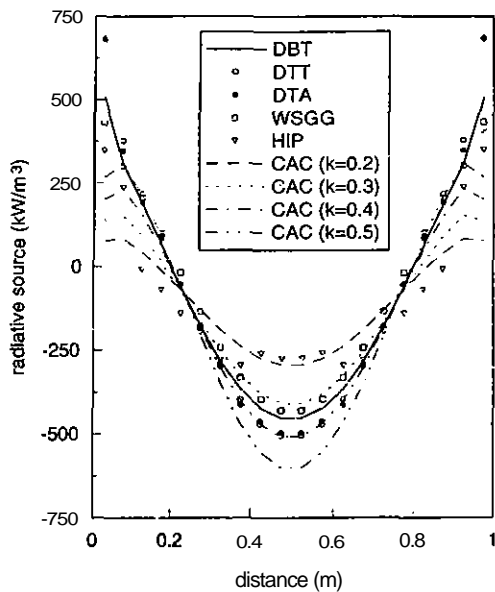


Figure 4. Radiative source across configuration A bounded by solid walls (emissivity = 0.25).

black walls none of the high-temperature radiation at the center of the slab is reflected back into the gas.

Qualitatively, the CAC solution with an absorption coefficient of approximately 0.3 predict the volumetric source variation reasonably well. This is especially so at the center of the slab, but there is an increasing error at the edges.

The HIP solution exhibits poor performance, underpredicting net emission at the center of the slab and underpredicting net absorption at the edges.

Although the WSGG solution follows the DBT solution closely across the path, the absolute relative error is large in regions of low net emission. This inflates the mean percentage error in both Figures 3 and 4. The total property solutions overpredict absorption at the edges of the slab and underpredict it at the center. However, they exhibit good accuracy in regions of low net emission. These methods are weakened by the modeling of absorption from wall radiation using a total absorptivity calculated from mean thermodynamic properties for each path.

### Configuration B with Solid Walls

When configuration B is applied between solid walls, the bulk of the gas is a net absorber of radiative energy. In the black wall case only one element adjacent to the walls is a net emitter—cf. Figure 5. The depth of emitting gas is slightly deeper for the low-emissivity walls, as shown in Figure 6. Due to the walls being at the highest temperature, high wall emissivity produces greater gas absorption than high wall reflectivity. Another feature of these hot wall configurations is that the greatest net absorption does not occur in the coolest region, but at points almost one-quarter of the total path length from each wall. This is due to the coolest region being farthest from the high-temperature walls and adjacent gas.

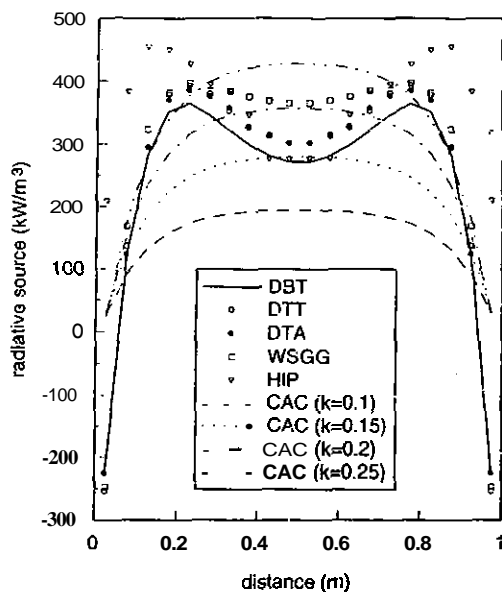
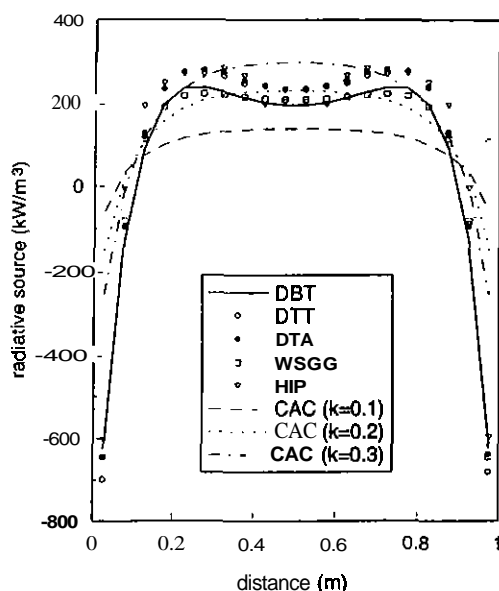


Figure 5. Radiative source across configuration B bounded by solid walls (emissivity = 1.0).



**Figure 6.** Radiative source across configuration B bounded by solid walls (emissivity = 0.25).

The CAC solutions fail to capture the double maximum of the volumetric source variation. For black walls they also fail to predict the net emission from the gas adjacent to the wall.

The HIP solution does capture the two maxima, but only predicts net emission from the gas adjacent to the wall for the gray wall case.

In contrast to configuration A between cool walls, the total property solutions produce lower mean percentage errors for high-emissivity walls. The reverse is true for the WSGG solution. All the solutions overestimate net absorption.

## CONCLUSIONS

A differential total absorptivity solution (DTA) to the radiative transfer equation has been assessed for application in the discrete transfer radiation model. The DTA solution explicitly addresses the source temperature dependence of absorption. Relative to the narrow-band solution (DBT), it provides the best representation of gas-gas radiation.

Both differential total property solutions and the weighted sum of gray gases solution produce good qualitative predictions for radiative intensity and volumetric sources for the configurations considered. Generally, the constant absorption coefficient (CAC) solution and the homogeneous isothermal path solution do not. Additionally, the most suitable absorption coefficient for the CAC solution is not known in advance of calculation.

However, all the approximate solutions, including the DTA, require improved treatment of solid-gas radiation.

With respect to computational effort, the WSGG solution is approximately an order of magnitude faster than the differential total property solutions, which are over two orders of magnitude faster than the DBT solution. Considering current levels of computing power, the greater accuracy offered by the DTA solution more

than compensates for the greater CPU penalty relative to the WSGG solution. Hence, the DTA solution is recommended for use in the discrete transfer radiation model when it is applied in nonuniform-property CFD heat transfer calculations.

## REFERENCES

1. F. C. Lockwood and N. G. Shah, A New Radiation Solution Method for Incorporation in General Combustion Prediction Procedures, *Eighteenth Symp. (Int.) on Combustion*, pp. 1405-1414, Combustion Institute, Pittsburgh, 1981.
2. M. G. Carvalho, P. Oliveira, and V. S. Semiao, A Three-Dimensional Modelling of an Industrial Glass Furnace, *J. Inst. Energy*, pp. 143-156, 1988.
3. A. S. Abbas and F. C. Lockwood, Prediction of Power Station Combustors, *Twenty-First Symp. (Int.) on Combustion*, pp. 285-292, Combustion Institute, 1986.
4. M. Fairweather, W. P. Jones, and R. P. Lindstedt, Predictions of Radiative Transfer from a Turbulent Reacting Jet in a Cross-Wind, *Combustion & Flame*, vol. 89, pp. 45-63, 1992.
5. T. K. Kim, J. A. Menart, and H. S. Lee, Nongray Radiative Gas Analysis Using the  $S-N$  Discrete Ordinates Method, *J. Heat Transfer*, vol. 113, pp. 946-952, 1991.
6. R. Viskanta and M. P. Menguc, Radiation Heat Transfer in Combustion Systems, *Prog. Energy Combustion Sci.*, vol. 13, pp. 97-160, 1987.
7. Tae-Ho Song, Comparison of Engineering Models of Nongray Behaviour of Combustion Products, *Int. J. Heat Mass Transfer*, vol. 36, no. 16, pp. 3975-3982, 1993.
8. P. Docherty and M. Fairweather, Predictions of Radiative Transfer from Nonhomogeneous Combustion Products Using the Discrete Transfer Method, *Combustion & Flame*, vol. 71, pp. 79-87, 1988.
9. R. Siegel and J. R. Howell, *Thermal Radiation Heat Transfer*, pp. 683-689, Hemisphere, Washington, DC, 1992.
10. N. W. Bressloff, J. B. Moss, and P. A. Rubini, Application of a New Weighting Set for the Discrete Transfer Radiation Model, *3rd European Conf. on Industrial Furnaces and Boilers*, Lisbon, Portugal, 1995.
11. J. Taine, A Line-by-Line Calculation of Low-Resolution Radiative Properties of  $\text{CO}_2$ - $\text{CO}$ -Transparent Nonisothermal Gaseous Mixtures up to 3000K, *J. Quant. Spectrosc. Radiat. Transfer*, vol. 30, no. 4, pp. 371-379, 1983.
12. W. L. Grosshändler, Radiative Heat Transfer in Nonhomogeneous Gases: A Simplified Approach, *Int. J. Heat Mass Transfer*, vol. 23, pp. 1447-1459, 1980.
13. M. F. Modest, The Weighted-Sum-of-Gray-Gases Model for Arbitrary Solution Methods in Radiative Transfer, *J. Heat Transfer*, vol. 113, pp. 650-656, 1991.
14. C. B. Ludwig, W. Malkmus, J. E. Reardon, and J. A. L. Thomson, *Handbook of Infrared Radiation from Combustion Gases*, NASA SP-3080, Scientific and Technical Information Office, Washington, DC, 1973.
15. D. K. Edwards, Molecular Gas Band Radiation, in *Advances in Heat Transfer*, Vol. 12, pp. 115-193, Academic Press, New York, 1976.
16. H. C. Hotteit and A. F. Sarofim, *Radiative Transfer*, pp. 247-252, McGraw-Hill, New York, 1967.
17. A. T. Modak, Radiation from Products of Combustion, *Fire Research*, vol. 1, pp. 339-361, 1979.
18. B. Leckner, Spectral and Total Emissivity of Water Vapour and Carbon Dioxide, *Combustion & Flame*, vol. 19, pp. 33-48, 1972.
19. G. L. Hubbard and C. L. Tien, Infrared Mean Absorption Coefficients of Luminous Flames and Smoke, *J. Heat Transfer*, vol. 100, pp. 235-239, 1978.

20. A. Soufiani, J. M. Hartman, and J. Taine, Validity of Band-Model Calculations for  $\text{CO}_2$  and  $\text{H}_2\text{O}$  Applied to Radiative Properties and Conductive-Radiative Transfer, *J. Quant. Spectrosc. Radiat. Transfer*, vol. 35, no. 3, pp. 243-257, 1985.
21. A. Soufiani and E. Djavdan, A Comparison between Weighted Sum of Gray Gases and Statistical Narrow-Band Radiation Models for Combustion Applications, *Combustion & Flame*, vol. 97, pp. 240-250, 1994.
22. J. S. Truelove, Zone Method for Radiative Heat Transfer Calculations, HTFS DR33, AERE, Harwell, Oxon, England, 1975.